A predictive model of radiation-related fibrosis based on the radiomic features of magnetic resonance imaging and computed tomography

Jian Wang[1], Rongjie Liu[2], Yu Zhao[3], Chonnipa Nantavithya[4], Hesham Elhalawani[5], Hongtu Zhu[6], Abdallah Sherif Radwan Mohamed[5], Clifton David Fuller[5], Danita Kannarunimit[4], Pei Yang[7], Hong Zhu[1]

[1]Department of Oncology, Xiangya Hospital, Central South University, Changsha, China; [2]Department of Statistics, Florida State University, Tallahassee, Florida, USA; [3]Unity Hospital, Rochester Region Health, Rochester, New York, USA; [4]Department of Medicine, Chulalongkorn University/King Chulalongkorn Memorial Hospital, Bangkok, Thailand; [5]Department of Radiation Oncology, MD Anderson Cancer Center, Houston, Texas, USA; [6]Department of Biostatistics, University of North Carolina at Chapel Hill, Chapel Hill, NC, USA; [7]Department of Radiotherapy, Hunan Cancer Hospital, Affiliate Tumor Hospital of Xiangya Medical School, Central South University, Key Laboratory of Translational Radiation Oncology of Hunan Province, Changsha, China

Contributions: (I) Conception and design: J Wang, P Yang, H Zhu; (II) Administrative support: H Zhu; (III) Provision of study materials or patients: P Yang; (IV) Collection and assembly of data: J Wang; (V) Data analysis and interpretation: R Liu; (VI) Manuscript writing: All authors; (VII) Final approval of manuscript: All authors.

Correspondence to: Hong Zhu. Department of Oncology, Xiangya Hospital, Central South University, Changsha 410008, China. Email: zhuhong0719@126.com; Pei Yang. Department of Radiotherapy, Hunan Cancer Hospital, Affiliate Hospital of Xiangya Medical School, Central South University, Key Laboratory of Translational Radiation Oncology of Hunan Province, Changsha 410013, China. Email: yangpei@hnca.org.cn.

Background: To establish a predictive model for the fibrotic level of neck muscles after radiotherapy by using radiomic features extracted from the magnetic resonance imaging (MRI) before and after radiotherapy and planning computed tomography (CT) in nasopharyngeal carcinoma patients.

Methods: A total of one hundred and eighty-six patients were finally enrolled in this study. According to the specific standard, all patients were divided into three different fibrosis groups. Regions of interests (ROI), including sternocleidomastoids (SCMs), trapezius (T), levator scapulae (LS), and scalenus muscles (S), were delineated manually and used for features extraction on IBEX. XGBoost, a machine learning algorithm, was used for the establishment of the prediction model. First, the patients were divided into training cohort (80%) and testing cohort (20%) randomly. Then the image features of CT or delta changes calculated from pre- and post-radiotherapy MRI images on each cohort constituted training and testing datasets. Then, based on the training dataset, a well-trained prediction model was produced. We used five-fold cross-validation to validate the predictive models. Afterward, the model performance was assessed on the 'testing' set and reported in terms of area under the receiver operating characteristic curve (AUC) under five scenarios: (I) only T1 sequence, (II) only T2 sequence, (III) only T1 post-contrast (T1 + C) sequence, (IV) Combination of all MRI sequences, (V) only CT.

Results: Most of the patients enrolled are male (73.1%), mean age was 47 years, receiving concurrent chemo-radiotherapy as the primary treatment (90.9%). By the end of the final follow-up, most of the patients were rated as mild fibrosis (60.8%). We found the prediction model based on the CT image features outperform all MRI features with an AUC of 0.69 and accuracy of 0.65. Contrarily, the model based on features from all MRI sequence showed lower AUC less than 0.5 and lower accuracy less than 0.6.

Conclusions: The prediction model based on CT radiomics features has better performance in the prediction of the grade of post-radiotherapy neck fibrosis. This might help guide radiotherapy treatment planning to achieve a better quality of life.

Keywords: Fibrosis; machine learning; nasopharyngeal carcinoma; quality of life

Introduction

Nasopharyngeal carcinoma is relatively rare worldwide. In 2018, 129,079 new cases of this malignancy were diagnosed, accounting for 0.7% of all cancers (1). Still, nasopharyngeal carcinomas are commonly diagnosed in Asia, especially in China [the crude incidence rate was 3.26/100,000 (2)]. Radiotherapy remains the standard treatment for these generally radiosensitive tumors and current estimates of 5-year overall survival after radiotherapy range from 66% to 83% (3). Given these promising survival rates, oncologists increasingly have focused on the quality of life of their patients. Radiation-related fibrosis is a typical late-onset complication of radiotherapy (4). This sequela may not arise until a few years after the end of the treatment and may progress or deteriorate further over time (4,5). Fibrosis can impair the functions of muscles in the head and neck and may thus restrict the opening of the mouth and jaw, motion in the shoulders, and rotation of the neck. Also, neck fibrosis may also cause cranial nerve palsy by compressing the hypoglossal nerve (6,7). All of these restrictions can interfere with eating, speaking, driving, self-care, and employment (5), severely impairing the quality of life. Radiation fibrosis is a multi-stage development process regulated by a variety of molecules, so it is difficult to design drugs that work at all stages. The current treatment strategies are mainly focused on limiting the aggravation of fibrosis, including topical emulsions (8), antioxidant therapies (9), hyperbaric oxygen therapy (10), adipose-derived stem cells (11) and some other therapies directly inhibiting the inflammatory mediators (12). The acupuncture and moxibustion therapy of traditional Chinese medicine also show a certain curative effect (13). However, the treatment options for radiation-related fibrosis are limited, and their therapeutic effects cannot sufficiently reverse the evolution and progression of fibrosis. Therefore, it is crucial to identify patients potentially at a high risk of fibrosis, as this will allow the application of preventive interventions to ensure optimal function and quality of life or minimize the side effects of treatment.

Fibrosis is characterized by an increase in tissue stiffness (i.e., loss of compliance), which can be detected by palpation. Accordingly, most studies have used hand palpation and clinician-based rating scales of fibrosis, including the Medical Research Council (MRC) (14), European Organization for Research and Treatment of Cancer/Radiation Therapy Oncology Group (EORTC/RTOG) (15), and Late Effects in Normal Tissues/Subjective, Objective, Management, and Analytic (LENT/SOMA) scoring systems (16). However, these scales are inevitably subjective, semiquantitative (17), and prone to interobserver error. Other studies have applied quantitative mechanical methods (18), quantitative electrical methods (19,20), ultrasound shear wave elastography (21), and magnetic resonance imaging (MRI) (22,23) to various parts of the body for fibrosis assessment. In the neck, tissue fibrosis may affect multiple tissue layers with considerable overlap. Currently, all of these changes cannot be detected using a single measurement technique, and even invasive biopsy is limited due to the ability to sample only specific microscopic points.

The field of radiomics is not based on information from images or single pathological tissue layers. Accordingly, this field differs from the traditional practice of subjecting medical images solely to visual interpretation (24). Radiomics exhibits tremendous promise as a comprehensive method of three-dimensional examination that enables the noninvasive profiling of multiple tissue layers (25). Nowadays, more and more researches begin to focus on the functional evaluation by using radiomics. A previous exploratory study succeeding in finding the relationship between the radiation dose to the masseter and the medial pterygoid and the variance of the MRI intensity of the radiation-induced trismus described by the radiomic textures (26). At the same time, a number of studies have shown the relationship between the image features and radiation-induced xerostomia and the integration of image features into the predictive model may improve the risk stratification of xerostomia (27-29). MRI is used widely in clinical workups for the pretreatment diagnosis and staging of nasopharyngeal carcinoma and as a conventional routine follow-up method. And every patient would perform planning CT scans before radiotherapy. In this study, therefore, we aimed to grope for if the radiomic features extracted from many types of MRI scans or CT could build a predictive model of radiation-related fibrosis.
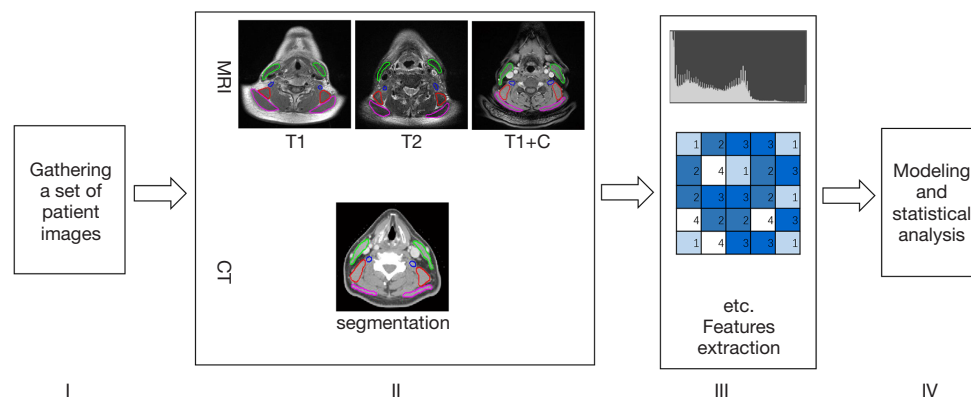
Figure 1 A workflow to produce a predictive model. These steps include gathering a set of patient images, segmentation of the region of interest (ROI) including four muscle, extracting a set of radiomics features from these ROIs, generating a predictive model and then perform the statistical analysis.

Methods

The workflow of this study is depicted in *Figure 1*. Specific contents and details in the process are described below.

Patient cohort

The study was conducted in accordance with the Declaration of Helsinki (as revised in 2013). The study was approved by Ethic Committee of the Hunan Cancer Hospital (No. 07 of 2020 Scientific Research Quick Review). The study is a retrospective study that examines the fait accompli of the past. Before the retrospective study, all the private information of patients will be anonymized, no direct contact with patients, no privacy of patients, the results of the study are only used for medical research, there is no risk to the patients included in the study. Based on the above, we applied for exemption from the informed consent of the subject and approved by the Ethic Committee.

For this study, we initially analyzed all MRI and CT data of 749 patients from the same institution in 2015, who received chemoradiation in 6–7 weeks. All MR images were obtained from a 1.5-T MRI system (GE sigma CV/i) during routine clinical practice. All photos were axial scans with the field of view of 30 cm, slice thickness of 5 mm, and slice spacing of 1 mm. CT images were acquired on GE LightSpeed RT (GEHW) with a peak tube voltage of 120 kVp and exposure of 200mAs. Images had 512×512 pixels, FOV of 550.0 mm × 550.0 mm, and a slice thickness of 5 mm.

The final analysis included the images, clinical factors,

and outcome data of the patients who met the following inclusion criteria: (I) initial treatment for pathologically confirmed nasopharyngeal carcinoma at a single institution in 2015; (II) no history of radiotherapy of neck and head because of other disease; (III) treated with static intensity-modulated radiation therapy (s-IMRT), step and shoot; (IV) availability of MR images collected at two points (before radiotherapy and up to 6 months post-treatment), including T1-weighted (T1), T1 post-contrast (T1 + C), and T2-weighted (T2) scans; (V) availability of planning CT images. Patients were excluded when they met the following criteria: (I) patients who could not be contacted at the follow-up time; (II) unavailability of MR images at each point or planning CT images; (III) poor image quality which is not sufficient for diagnosis and analysis. The specific screening process is shown in *Figure 2*.

Clinical factors

The patient's clinical parameters were obtained through a retrospective review and are presented systematically in *Table 1*. The median follow-up duration was 18 months (range, 11–22 months). The patients were asked about the presence of four symptoms: (I) discomfort in the neck (self-rated on a scale of 0–10), (II) experience of late facial edema after treatment (yes or no, if yes, how long did it regress), (III) experience of upper limb pain after treatment (yes or no, if yes, the severity and is there any treatment), and (IV) restricted head rotation during activities of daily living (yes or no, if yes, the degree of limitation and how long does it last). Based on these symptoms and physical signs, all
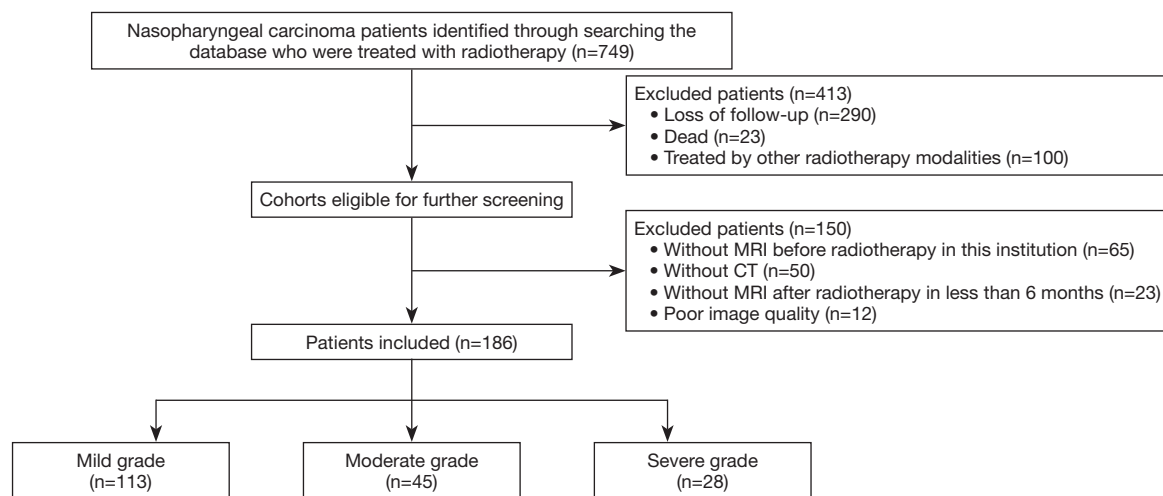
Figure 2 Flow diagram for patient selection in our study.

patients were divided into three groups: mild, moderate, and severe fibrosis. Specific standards are listed in *Table 2*.

Lesion segmentation

Lesion segmentation was performed using The Imaging Biomarker Explorer (IBEX) software package, version 1.0 (30). An experienced clinical oncologist used the IBEX software to contour the ROIs manually on each type of MRI sequence (T1, T1 + C, and T2) and CT for each patient. Later, the contoured ROI would be reviewed by another experienced radiologist. It has been reported that muscle fibrosis develops before skin fibrosis (31). Based on this theory, the ROI was drawn to include sternocleidomastoids (SCMs), trapezius (T), levator scapulae (LS), and scalenus muscles (S). The ROI was divided horizontally into two parts based on the level of the cricoid cartilage, which received a different radiation dose during radiotherapy. It is worth reminding that we contoured four ROIs above the cricoid cartilage on CT because of the loss of part images.

Extraction and calculation of radiomic features

IBEX was used to extract image features from pre- and post-radiotherapy MRI images or planning CT images. Categorization according to specific standards (*Table 2*) was used to label the image features like three different groups. As shown in *Table 3*, the textural features calculated in this study can be organized into 10 categories. Two processing

methods were applied, including Resample Voxel Size and Butterworth Smooth (32), which lessened the image noise. Assigning different parameters to every textural feature, and a total of 190 texture features were acquired for each sequence of the MRI at every time points and 1,767 for CT. The magnitude of change of each feature was computed as follows: delta change = (post – pre)/pre, being used for MRI feature modeling, where post and pre correspond to the measurements after and before radiation therapy, respectively. Changes from the first time to the second time in radiomics features, called delta-radiomics, have been proved to improved model for predicting the prognosis of patients combined with clinical factors and radiomic characteristics (33). On the meanwhile, features acquired on CT were directly used for modeling on the next step.

Feature modeling

In reality, many features have high noise and may lead to overfitting or classification errors in feature modeling. Not all image features can be conductive to grade the severity of neck fibrosis after radiotherapy. Features were selected for the prediction performance in terms of the AUC (>0.6). Meanwhile, XGBoost, a Gradient Tree Boosting regularization form (34), could identify a subset of essential features to avoid feature redundancy for feature modeling in the course of calculation. Previous studies have reported that XGBoost showed lower test error rate and the larger AUC in comparison with logistic regression analysis and

4730

Wang et al. Radiomics for prediction of radiation-related fibrosis

Table 1 Patient's clinical and dosimetric parameters

Clinical factors	N=186	Training cohort				Testing cohort			
		Mild	Moderate	Severe	P	Mild	Moderate	Severe	P
SEX					0.972				0.645
Male	136	67	24	18		17	6	4	
Female	50	23	12	4		6	3	2	
AGE (years)					0.005				0.273
≥65	8	1	2	3		1	1	0	
<65	178	89	34	19		22	8	6	
T stage					0.935				0.852
T1	19	10	3	2		2	1	1	
T2	59	28	14	5		7	4	1	
T3	60	30	10	8		7	2	3	
T4	48	22	9	7		7	2	1	
N stage					0.398				0.714
N0	4	1	1	1		1	0	0	
N1	28	13	6	3		3	1	2	
N2	112	58	20	11		14	5	4	
N3	42	18	9	7		5	3	0	
M stage					0.03				0.524
M0	178	88	36	18		22	9	5	
M1	8	2	0	4		1	0	1	
Clinical stage					0.222				0.672
I	2	0	1	0		0	1	0	
II	11	6	2	1		2	0	0	
III	91	45	18	10		11	4	3	
IVa	74	37	15	7		9	4	2	
IVb	8	2	0	4		1	0	1	
Concurrent chemoradiotherapy					0.641				0.687
No	17	9	4	1		2	1	0	
Yes	169	81	32	21		21	8	6	

The 7th American Joint Committee on Cancer (AJCC) TNM staging manual was used to stage the patients.

other machine learning approaches, including decision tree, random forest, and support vector machine (35). It leads us to propose using this method for the establishment of the prediction model of radiation-related fibrosis. First, the subjects included were divided into five folds which was consistent with the proportion of the three fibrotic groups in the overall cohort randomly. Then four folds constituted the training cohort, and the remaining one constituted the testing cohort. The modeling was done based on the selected image features delta changes on the MRI images

Table 2 Categorization of 186 patients according to muscle fibrosis in the neck after treatment

Level	Conditions (meet any of the following)
Mild	(I) Rating: 0–4 points
	(II) No facial edema
	(III) No upper limb pains
	(IV) Neck activity is unrestricted
Moderate	(I) Rating: 4–6 points
	(II) Late facial edema (regress within 3 months)
	(III) Mild upper limb pain (no treatment)
	(IV) Neck activity is slightly limited
Severe	(I) Rating: 7–10 points
	(II) Late facial edema, lasting more than 3 months
	(III) Severe upper limb pain, or needing medical intervention
	(IV) Neck activity is significantly limited or duration >6 months

Categorization into a specific group required the patient to meet any of the above criteria.

that were calculated in the previous step or the features extracted from CT on the cohort. Next, XGBoost was used to generate a well-trained prediction model based on the training image dataset. Though a lack of independent external validation, we do perform five-fold cross-validation (internal validation), which is identified to be an effective way to build patient-specific predictions without bias (36). Finally, we compared the prediction performance under five scenarios: (I) only the T1 sequence; (II) only the T2 sequence; (III) only the T1 + C sequence; (IV) combination all the MRI sequences; (V) only the CT. The performance of the predictive model was then assessed using the testing image set, and the results are reported in terms of the mean AUC.

Results

Patients cohort and selected features

As shown in *Figure 2*, lastly, a total of 186 patients were finally enrolled for further analysis. The patients include was divided into training cohort (80.0%) and testing cohort (20%) randomly. The patient sample was predominantly male (73.1%), with a mean age of 47 years. The majority had locally advanced disease (93.0%) and had received concurrent chemoradiotherapy as the primary treatment (90.9%). By the end of the final follow-up, most patients were classified as having mild fibrosis (60.8%). There are no

significant differences among the fibrosis groups for all the factors except age (P=0.005) and metastasis stage (P=0.03) of the patients in the training cohort. Detailed clinical parameters are depicted in *Table 1*. As shown in *Figure 3*, fibrosis degree has nothing to do with the lymph node stage. We performed spearman relativity analysis between these two variables (P=0.613, r_s=0.029).

A total of 139 textures from T1 sequence, 138 features from T2 sequence and 157 features from T1 + C sequence were used for feature modeling and 749 features for CT. As shown in *Table 3*, extracted features include first-order, second-order and higher-order characteristic, which can be further grouped into ten categories. Shape features, Neighbor Intensity Difference features, Intensity Histogram Gaussian Fit features, Intensity histogram features, Intensity Direct features (37), Gray Level Co-occurrence Matrix features, Gray Level Run Length Matrix features (38), and Gradient Orient Histogram features (39) were enrolled in this study.

Feature modeling

The radiomics signatures based on MRI images or CT images performed well in predicting the degree of fibrosis after radiotherapy. Values of AUC, accuracy, sensitivity and specificity of the five scenarios are as shown in *Table 4*. When predicting three different fibrosis groups, we found the model based on the CT image features showed better

4732

Wang et al. Radiomics for prediction of radiation-related fibrosis

Table 3 The features used in this study and related preprocessing methods

Category	Feature	Preprocess
Gradient Orient Histogram	Inter Quartile Range	Resample Voxel Size
	Kurtosis	
	Mean Absolute Deviation	
	Median Absolute Deviation	
	Percentile	
	Percentile Area	
	Quantile	
	Range	
	Skewness	
Gray Level Co-occurrence Matrix 25	Auto Correlation	Resample Voxel Size
	Cluster Prominence	
	Cluster Shade	
	Cluster Tendency	
	Contrast	
	Correlation	
	Difference Entropy	
	Dissimilarity	
	Energy	
	Entropy	
	Homogeneity	
	Homogeneity2	
	InformationMeasureCorr1	
	InformationMeasureCorr2	
	Inverse Diff Moment Norm	
	Inverse Diff Norm	
	Inverse Variance	
	Max Probability	
	Sum Average	
	Sum Entropy	
	Sum Variance	
	Variance	

Table 3 (*Continued*)

Table 3 (*Continued*)

Category	Feature	Preprocess
Gray Level Co-occurrence Matrix 3	Auto Correlation	Resample Voxel Size
	Cluster Prominence	
	Cluster Shade	
	Cluster Tendency	
	Contrast	
	Correlation	
	Difference Entropy	
	Dissimilarity	
	Energy	
	Entropy	
	Homogeneity	
	Homogeneity2	
	InformationMeasureCorr1	
	InformationMeasureCorr2	
	Inverse Diff Moment Norm	
	Inverse Diff Norm	
	Inverse Variance	
	Max Probability	
	Sum Average	
	Sum Entropy	
	Sum Variance	
	Variance	
Gray Level Run Length Matrix25	Gray Level Nonuniformity	Resample Voxel Size, Butterworth Smooth
	High Gray Level Run Emphasis	
	Long Run Emphasis	
	Long Run High Gray Level Emphasis	
	Long Run Low Gray Level Emphasis	
	Low Gray Level Run Emphasis	
	Run Length Nonuniformity	

Table 3 (*Continued*)

Table 3 (*Continued*)

| Category	Feature	Preprocess
	Run Percentage	
	Short Run Emphasis	
	Short Run High Gray Level Emphasis	
	Short Run Low Gray Level Emphasis	
Intensity Direct	Energy	Resample Voxel Size
	Energy Norm	
	Global Entropy	
	Global Max	
	Global Mean	
	Global Median	
	Global Min	
	Global Std	
	Global Uniformity	
	Inter Quartile Range	
	Kurtosis	
	Local Entropy Max	
	Local Entropy Mean	
	Local Entropy Median	
	Local Entropy Min	
	Local Entropy Std	
	Local Range Max	
	Local Range Mean	
	Local Range Median	
	Local Range Min	
	Local Range Std	
	Local Std Max	
	Local Std Mean	
	Local Std Median	
	Local Std Min	
	Local Std Std	
	Mean Absolute Deviation	
	Median Absolute Deviation	
	Percentile	

Table 3 (*Continued*)

Table 3 (*Continued*)

Category	Feature	Preprocess
	Quantile	
	Range	
	Root Mean Square	
	Skewness	
Intensity Histogram	Inter Quartile Range	Resample Voxel Size, Butterworth Smooth
	Kurtosis	
	Mean Absolute Deviation	
	Median Absolute Deviation	
	Percentile	
	Percentile Area	
	Quantile	
	Range	
	Skewness	
Neighbor Intensity Difference 25	Busyness	Resample Voxel Size, Butterworth Smooth
	Coarseness	
	Complexity	
	Contrast	
	Texture Strength	
Neighbor Intensity Difference 3	Busyness	Resample Voxel Size, Butterworth Smooth
	Coarseness	
	Complexity	
	Contrast	
	Texture Strength	
Shape	Compactness1	–
	Compactness2	
	Convex	
	Convex Hull Volume	
	Convex Hull Volume 3D	
	Mass	
	Max3D Diameter	
	Mean Breadth	

Table 3 (*Continued*)

Table 3 (*Continued*)

Category	Feature	Preprocess
	Number of Objects	
	Number of Voxel	
	Orientation	
	Roundness	
	Spherical Disproportion	
	Sphericity	
	Surface Area	
	Surface Area Density	
	Volume	
	Voxel Size	
Intensity Histogram Gaussian Fit	Gaussian Amplitude	Resample Voxel Size
	Gaussian Area	
	Gaussian Mean	
	Gaussian Std	
	Hist Area	
	Number of Gaussian	
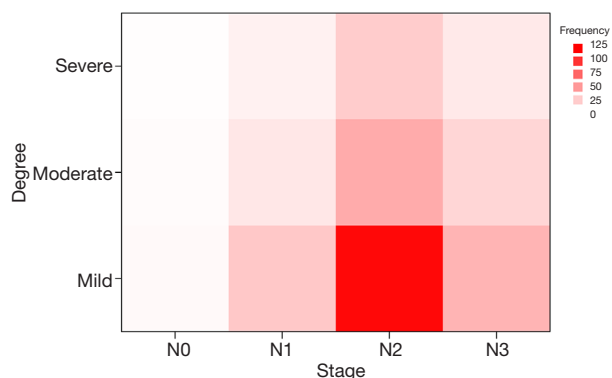
Figure 3 A hotspot map of the relationship between lymph node stage and the degree of fibrosis.

performance, with an AUC of 0.69 and accuracy of 0.65 compared to that models of T1, T2, T1 + C, and combine all three sequences show lower AUC (all is 0.49) and lower accuracy (0.56, 0.55, 0.57, 0.58).

Discussion

In this study, we developed predictive models of radiation-related fibrosis based on the radiomic features of MRI and CT. These features exhibited predictive power to a certain extent. To our best knowledge, our group was the first to use the radiomic features of MRI and CT to predict the grade of radiation-related fibrosis on the neck. Additionally, we proposed a more practical standard for fibrosis level, including symptoms and physical signs.

Notably, the features extracted from CT outperformed all other feature changes from commonly used MRI scans, including T1, T2, and T1 + C, in terms of AUC values and accuracy. Compared with CT, MRI has the advantage of showing soft tissue lesions better and providing muscle-specific measurements. Researchers have previously identified a close relationship between MRI features and the severity of radiation-induced fibrosis (40). However, we did find that image features from CT have higher accuracy in predicting the degree of fibrosis after radiotherapy. Despite we only contoured four ROIs on CT images compared to eight ROIs on MRI, more features were extracted from CT. Besides, the type of acquisition noise, enhancement status, and image reconstruction algorithm have different effects on MRI imaging characteristics, especially in a retrospective study (41). To our knowledge, no standardized MRI method has been developed for the purpose of head and neck scanning or radiomics. Therefore, the effects of various MRI factors on the image data cannot yet be avoided. On the other hand, despite no existing studies have correlated clinically rated neck fibrosis with CT findings, previous studies have found textural image features extracted from CT are highly correlated with the severity of pulmonary fibrosis (42) and could discriminate between patients with and those without radiation pneumonitis (43). Moreover, the previous study has used CT texture changes for distinguishing radiation-induced fibrosis from tumor recurrence for lung cancer (44).

Despite the advantages of this approach, our research had some limitations. First, standard protocols for fibrosis grading included patient self-ratings, which inevitably led to subject bias. Second, the current radiomic analysis protocol involves complex computational steps with frequent human interactions and a potentially time-consuming analytical process and may be challenging to include in daily clinical practice. Currently, this post-processing process includes multiple steps and calculations and requires

Table 4 The performance of the predictive model using the XGBoost

Modality	AUC	Accuracy	Degree	Sensitivity (%)	Specificity (%)
T1	–	–	(I) Mild	81.39	20.10
	0.49	0.56	(II) Moderate	13.33	83.87
	–	–	(III) Severe	3.33	96.20
T2	–	–	(I) Mild	84.04	6.71
	0.49	0.55	(II) Moderate	4.00	88.45
	–	–	(III) Severe	3.00	96.60
T1 + C	–	–	(I) Mild	81.35	19.29
	0.49	0.57	(II) Moderate	17.33	83.34
	–	–	(III) Severe	0.20	97.73
T1 + T2 + T1 + C		–	(I) Mild	85.09	14.52
	0.49	0.58	(II) Moderate	13.33	88.93
	–	–	(III) Severe	3.00	96.58
CT	–	–	(I) Mild	98.74	2.09
	0.69	0.65	(II) Moderate	2.15	98.66
	–	–	(III) Severe	0.00	100.00

AUC, area under the curve; T1, T1-weighted scans; T1 + C, T1 post-contrast cans; T2, T2-weighted scans; CT, computed tomography.

approximately 60 minutes per patient (45). But we believe that as technological innovation and the optimization of the algorithm, it will be less time-consuming in the future. Moreover, our study did not distinguish between radiation-induced fibrosis and residual or recurrent tumor. The residual tumor remained after treatment in nearly 7–13% of nasopharyngeal carcinoma cases (46). A future prospective study should incorporate data from dynamic contrast-enhanced MRI, the primary choice for the diagnosis of neck fibrosis after radiotherapy for nasopharyngeal carcinoma, given its ability to identify tumor residue, recurrence, and fibrosis (47). Finally, our analysis was based on a retrospective design and data from a single center. Our model requires validation through a prospective multicenter trial with a larger study cohort.

Conclusions

In conclusion, we constructed a predictive, non-invasive, inexpensive, and highly patient-specific model of radiation-related fibrosis that does not affect existing clinical activities. This model requires further optimization, but it does contribute to the decision-making of the radiation treatment. Oncologists may use this model to compare

the potential effects of different therapeutic regimens on the grade of radiation-related fibrosis and could thus individually tailor treatments to minimize the side reaction by adjusting the dose prescription on the neck. Furthermore, our model may inform studies of radiation-related injuries in other body regions. In the future, we aim to develop the model further to enable direct predictions of the effects of radiation-related fibrosis on the quality of life.

Acknowledgments

Footnote

Data Sharing Statement: Available at http://dx.doi.org/10.21037/tcr-20-751

4736

Wang et al. Radiomics for prediction of radiation-related fibrosis

Conflicts of Interest: All authors have completed the ICMJE uniform disclosure form (available at http://dx.doi.org/10.21037/tcr-20-751). The authors have no conflicts of interest to declare.

Ethical Statement: The authors are accountable for all aspects of the work in ensuring that questions related to the accuracy or integrity of any part of the work are appropriately investigated and resolved. The study was conducted in accordance with the Declaration of Helsinki (as revised in 2013). The study was approved by Ethic Committee of the Hunan Cancer Hospital (No. 07 of 2020 Scientific Research Quick Review). The study is a retrospective study that examines the fait accompli of the past, and all the private information of patients will be anonymized, no direct contact with patients, no privacy of patients. Based on the above, we applied for exemption from the informed consent of the subject and approved by the Ethic Committee.

Open Access Statement: This is an Open Access article distributed in accordance with the Creative Commons Attribution-NonCommercial-NoDerivs 4.0 International License (CC BY-NC-ND 4.0), which permits the non-commercial replication and distribution of the article with the strict proviso that no changes or edits are made and the original work is properly cited (including links to both the formal publication through the relevant DOI and the license). See: https://creativecommons.org/licenses/by-nc-nd/4.0/.

References

1. Bray F, Ferlay J, Soerjomataram I, et al. Global cancer statistics 2018: GLOBOCAN estimates of incidence and mortality worldwide for 36 cancers in 185 countries. CA Cancer J Clin 2018;68:394-424.
2. Chen WQ, Li H, Sun KX, et al. Report of Cancer Incidence and Mortality in China, 2014. Zhonghua Zhong Liu Za Zhi 2018;40:5-13.
3. Zhao Y, Shen L, Huang X, et al. Prognostic analysis of patients with locally advanced nasopharyngeal carcinoma following intensity modulated radiation therapy. Oncol Lett 2018;15:4445-50.
4. Hirota S, Tsujino K, Oshitani T, et al. Subcutaneous fibrosis after whole neck irradiation. Int J Radiat Oncol Biol Phys 2002;52:937-43.
5. Zheng Y, Han F, Xiao W, et al. Analysis of late toxicity in

nasopharyngeal carcinoma patients treated with intensity modulated radiation therapy. Radiat Oncol 2015;10:17.
6. Kong L, Lu JJ, Liss AL, et al. Radiation-Induced Cranial Nerve Palsy: a Cross-Sectional Study of Nasopharyngeal Cancer Patients After Definitive Radiotherapy. Int J Radiat Oncol Biol Phys 2011;79:1421-7.
7. Lin YS, Jen YM, Lin JC. Radiation related cranial nerve palsy in patients with nasopharyngeal carcinoma. Cancer 2002;95:404-9.
8. Menêses AG, Reis PEDD, Guerra ENS, et al. Use of trolamine to prevent and treat acute radiation dermatitis: a systematic review and meta-analysis. Rev Lat Am Enfermagem 2018;26:e2929.
9. Lin SL, Chen RH, Chen YM, et al. Pentoxifylline attenuates tubulointerstitial fibrosis by blocking Smad3/4-activated transcription and profibrogenic effects of connective tissue growth factor. J Am Soc Nephrol 2005;16:2702-13.
10. Borab Z, Mirmanesh MD, Gantz M, et al. Systematic Review of Hyperbaric Oxygen Therapy for the Treatment of Radiation-Induced Skin Necrosis. J Plast Reconstr Aesthet Surg 2017;70:529.
11. Borovikova AA, Ziegler ME, Banyard DA, et al. Adipose-Derived Tissue in the Treatment of Dermal Fibrosis. Ann Plast Surg 2018;80:297-307.
12. Xavier S, Piek E, Fujii M, et al. Amelioration of Radiation-induced Fibrosis. J Biol Chem 2004;279:15167-76.
13. Yang Y, Guo H, Wang L. Clinical observation on acupuncture therapy and massage therapy of fibrosis in patients with nasopharyngeal carcinoma after radiotherapy. China Practical Medicine 2010;29:27-28.
14. Dische S. The uniform reporting of treatment-related morbidity. Semin Radiat Oncol 1994;4:112.
15. Cox JD, Stetz J, Pajak TF. Toxicity criteria of the Radiation Therapy Oncology Group (RTOG) and the European Organization for Research and Treatment of Cancer (EORTC). Int J Radiat Oncol Biol Phys 1995;31:1341-6.
16. Pavy JJ, Denekamp J, Letschert J, et al. EORTC Late Effects Working Group. Late effects toxicity scoring: the SOMA scale. Int J Radiat Oncol Biol Phys 1995;31:1043-7.
17. Leung SF, Zheng Y, Choi CY, et al. Quantitative measurement of post-irradiation neck fibrosis based on the young modulus: description of a new method and clinical results. Cancer 2002;95:656-62.
18. Guy RH. Handbook of non-invasive methods and the skin. J Control Release 1995;1:102.
19. Paulsen KD, Osterman KS, Hoopes PJ. In vivo

electrical impedance spectroscopic monitoring of the progression of radiation-induced tissue injury. Radiat Res 1999;152:41-50.

20. Osterman KS, Hoopes PJ, DeLorenzo C, et al. Non-invasive assessment of radiation injury with electrical impedance spectroscopy. Phys Med Biol 2004;49:665-83.

21. Bercoff J, Tanter M, Fink M. Supersonic shear imaging: a new technique for soft tissue elasticity mapping. IEEE Trans Ultrason Ferroelectr Freq Control 2004;51:396-409.

22. Wang J, Malik N, Yin M, et al. Magnetic resonance elastography is accurate in detecting advanced fibrosis in autoimmune hepatitis. World J Gastroenterol 2017;23:859

23. Hu G, Zhang X, Liang W, et al. Assessment of liver fibrosis in rats by MRI with apparent diffusion coefficient and T1 relaxation time in the rotating frame. J Magn Reson Imaging 2016;43:1082-9.

24. Gillies RJ, Kinahan PE, Hricak H. Radiomics: Images are more than pictures, they are data. Radiology 2016;278:563-77.

25. Lambin P, Rios-Velazquez E, Leijenaar R, et al. Radiomics: Extracting more information from medical images using advanced feature analysis. Eur J Cancer 2012;48:441-6.

26. Thor M, Tyagi N, Hatzoglou V, et al. A magnetic resonance imaging-based approach to quantify radiation-induced normal tissue injuries applied to trismus in head and neck cancer. Phys Imaging Radiat Oncol 2017;1:34-40.

27. Gabryś HS, Buettner F, Sterzing F, et al. Design and Selection of Machine Learning Methods Using Radiomics and Dosiomics for Normal Tissue Complication Probability Modeling of Xerostomia. Front Oncol 2018;8:35.

28. van Dijk LV, Thor M, Steenbakkers RJHM, et al. Parotid gland fat related magnetic resonance image biomarkers improve prediction of late radiation-induced xerostomia. Radiother Oncol 2018;128:459-66.

29. Sheikh K, Lee SH, Cheng Z, et al. Predicting acute radiation induced xerostomia in head and neck Cancer using MR and CT Radiomics of parotid and submandibular glands. Radiat Oncol 2019;14:131.

30. Zhang L, Fried DV, Fave XJ, et al. IBEX: an open infrastructure software platform to facilitate collaborative work in radiomics. Med Phys 2015;42:1341-53.

31. Li J, Wang RS, Liu WQ, et al. Cervical fibrosis and its influencing factors in patients with nasopharyngeal carcinoma after radiotherapy. Chin J Radiol Med Protection 2005;3:253-5.

32. Dogra A, Bhalla P. Image Sharpening By Gaussian And Butterworth High Pass Filter. Biomed Pharmacol J 2014;2:707-13.

33. Fave X, Zhang L, Yang J, et al. Delta-radiomics features for the prediction of patient outcomes in non–small cell lung cancer. Sci Rep 2017;7:588.

34. Liu L, Yu Y, Fei Z, et al. An interpretable boosting model to predict side effects of analgesics for osteoarthritis. BMC Syst Biol 2018;12:105.

35. Lee HC, Yoon HK, Nam K, et al. Derivation and validation of machine learning approaches to predict acute kidney injury after cardiac surgery. J Clin Med 2018;7:322.

36. Simon RM, Subramanian J, Li MC, et al. Using cross-validation to evaluate predictive accuracy of survival risk classifiers based on high-dimensional data. Brief Bioinform 2011;12:203-14.

37. Haralick RM, Shanmugam K, Dinstein I. Textural features for image classification. IEEE 1973;6:610-1.

38. Galloway MM. Texture analysis using gray level run lengths. Comput Graph Image Process 1975;2:172-9.

39. Li B, Cheng K, Yu Z. Histogram of Oriented Gradient Based Gist Feature for Building Recognition. Comput Intell Neurosci 2016;2016:6749325.

40. Hoeller U, Bonacker M, Bajrovic A, et al. Radiation-induced plexopathy and fibrosis: Is magnetic resonance imaging the adequate diagnostic tool? Strahlenther Onkol 2004;180:650-4.

41. Qian L, Zhaoxiang Y. The application of imaging in tumor research. Chin J Oncol 2018;11:801-4.

42. Caban JJ, Yao J, Bagci U, et al. Monitoring pulmonary fibrosis by fusing clinical, physiological, and computed tomography features. Conf Proc IEEE Eng Med Biol Soc 2011;2011:6216-9.

43. Cunliffe A, Armato SG, Castillo R, et al. Lung Texture in Serial Thoracic Computed Tomography Scans: Correlation of Radiomics-based Features With Radiation Therapy Dose and Radiation Pneumonitis Development. Int J Radiat Oncol Biol Phys 2015;91:1048-56.

44. Mattonen SA, Palma DA, Haasbeek CJA, et al. Early prediction of tumor recurrence based on CT texture changes after stereotactic ablative radiotherapy (SABR) for lung cancer. Med Phys 2014;41:033502.

45. Kickingereder P, Neuberger U, Bonekamp D, et al. Radiomic subtyping improves disease stratification beyond key molecular, clinical, and standard imaging characteristics in patients with glioblastoma. Neuro Oncology 2018;20:848-57.

46. Su D, Jin G, Xie D, et al. Identification of local recurrence

4738

Wang et al. Radiomics for prediction of radiation-related fibrosis

and radiofibrosis by computed tomography perfusion on nasopharyngeal carcinoma after radiotherapy. Can Assoc Radiol J 2010;61:265-70.

47. Mao J, Shen J, Yang Q, et al. Intravoxel incoherent motion

MRI in differentiation between recurrent carcinoma and postchemoradiation fibrosis of the skull base in patients with nasopharyngeal carcinoma. J Magn Reson Imaging 2016;44:1556-64.